Ultrafast dynamics of hot electrons and holes in copper: Excitation, energy relaxation, and transport effects

E. Knoesel, A. Hotzel, and M. Wolf
Fritz-Haber-Institut der MPG, Faradayweg 4-6, D-14195 Berlin, Germany
(Received 24 December 1997)

Time-resolved two-photon photoemission (2PPE) at various photon energies is used to investigate the relaxation dynamics of hot electrons in Cu(111), applying auto- and cross-correlation techniques. The relaxation times vary from 250 fs at 0.1 eV above the Fermi level to 20 fs at 2 eV and show a strong wavelength dependence in the vicinity of the *d*-band feature in the 2PPE spectra. Electrons not directly excited from the *d* band exhibit a much longer relaxation time than *d*-band electrons excited to the same intermediate-state energy. We attribute these apparently longer lifetimes to a delayed electron generation via Auger decay of *d*-band holes. Based on a band structure calculation, a simulation of the ballistic transport effect and its implication on the observed electron relaxation dynamics is presented for the three low-index copper surfaces. These observations suggest that *d*-band holes have a substantially longer lifetime than excited *sp*-band electrons of the corresponding excitation energy.
[S0163-1829(98)03720-5]

I. INTRODUCTION

In recent years the investigation of photochemical and related processes on surfaces, like desorption induced by electronic transition (DIET),[1–3] has led to a deeper understanding of the underlying mechanisms and elementary processes. At metal surfaces the first step of photochemical reactions is predominantly the generation of photoexcited ''hot'' electrons in the substrate, which may subsequently diffuse to the surface and attach to the adsorbed molecule to form a short-lived (typically <10 fs) negative ion resonance (see Fig. 1). During the lifetime of this adsorbate resonance, the necessary energy for a bond-breaking process can be transferred to the relevant reaction coordinate. This process is generally discussed within the Menzel-Gomer-Redhead (MGR) model[4,5] or Antoniewicz model.[6] In the framework of these models, the desorption cross section *per excitation* of the adsorbate is determined by the potential energy surfaces of the ground and excited state and by the lifetime of the latter. In order to determine the overall cross section *per absorbed photon*, however, the temporal evolution of the hot electron energy distribution at the surface as well as the attachment probability to the adsorbate must be known.

While the nascent hot electron distribution is determined by the band structure of the substrate and the inter- and intraband transition probabilities, its temporal evolution is strongly affected by the various relaxation and scattering processes in the substrate. Hot electron relaxation in metals occurs on an ultrashort time scale (<1 ps) where excited electrons lose their energy mainly through scattering events with electrons or phonons, whereas radiative decay takes place on a much longer time scale (>1 ns). For excess energies above ~ 100 meV, the dominant energy relaxation process for a hot electron is scattering with a ''cold'' electron below the Fermi level, because the energy transfer in electron-phonon scattering is only 15 meV [for Cu (Refs. 7 and 8)] in average. For *e-e* scattering the available phase space determines the dependence of electron lifetime on excess energy, which is theoretically described by the Fermi liquid theory.[9,10] However, these *e-e* scattering events (as well as the relaxation of the photogenerated hot holes) lead to additional excited (secondary) electrons, which dominate the hot electron distribution especially at low $E-E_{\mathrm{Fermi}}$.[11] Finally, the hot electron distribution in the near-surface region is also affected by the hot electron transport into the bulk.

At very high densities of excited electrons (when using intensive femtosecond laser pulses of typically >1 mJ/cm^2 absorbed laser fluence, ~ 100 fs pulse width), scattering processes between the excited hot electrons lead to a fast thermalization of the hot electron distribution. The relaxation dynamics can then be approximately described by a two-temperature model, i.e., by the temperatures of the electrons and the lattice.[12,13] Experimentally, the time scales for electron thermalization (the buildup of an electronic temperature) and the energy transfer from the electron distribution to the

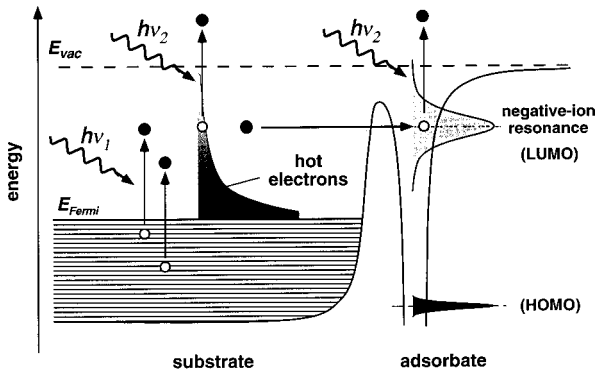

FIG. 1. Upon irradiation with laser light ($h\nu_1$), electron-hole pairs are generated in the substrate. Excited electrons of suitable energy can form a negative-ion resonance at the adsorbate. In 2PPE the hot electron energy distribution is probed by a second laser pulse ($h\nu_2$).

phonon bath were investigated mainly for noble metals using optical methods like transient reflectivity changes,[14–16] surface plasmon excitation,[17,18] and second-harmonic generation.[19,20] In a more recent time-resolved two-photon photoemission (2PPE) experiment Fann *et al.*[21,22] analyzed the temporal evolution of the hot electron distribution around the Fermi level in gold films and found that the electron thermalization is only partially completed before energy transfer to the lattice occurs. Interestingly, at this high density of excited electrons, the desorption dynamics is also different and results in a nonlinear dependence of the desorption yield on laser fluence.[12,23–25] This can be explained by multiple adsorbate excitation via electron attachment [desorption induced by multiple electronic transitions[26] (DIMET)].

In this paper we present time-resolved experiments on a Cu(111) surface, which were performed at low densities of excited electrons ($<2\times10^{18}$ cm^{-3}), where scattering between excited electrons is negligible and, therefore, the hot electron distribution is *not thermalized*. The first time-resolved 2PPE experiments on copper were performed by Schmuttenmaer *et al.*,[27] while more recently the electron dynamics on copper surfaces was investigated by several groups.[28–32] The relaxation dynamics at the low-index copper surfaces was investigated by Ogawa *et al.*[31] with excellent temporal resolution, whereby a pronounced crystal face dependence of the relaxation times was observed. Moreover, the electron relaxation dynamics was found to be slower than predicted by Fermi liquid theory (up to a factor of 5). Assuming a shorter screening length, the experimental data could be partially reproduced in an electron lifetime calculation based on the Cu band structure, which included the crystal face dependence of the phase space for *e*-*e* scattering events. This calculation, however, could not account for the observed crystal face dependence. Besides, it was found by two groups[30,32,33] that at certain electron excess energies the relaxation times in copper depend on photon energy; i.e., a correlation of the relaxation times with the *d*-band edge was observed. However, the authors differ in their interpretations of this phenomenon.

In this publication, we focus mainly on two effects, namely, the excitation mechanisms and the ballistic transport of the hot electrons and their respective influences on the experimentally observed relaxation times. By the results of our time-resolved experiments, the excitation pathway for a pronounced *d*-band feature can be identified as an instantaneous two-photon transition. The apparent dependence of the relaxation times on photon energy can be rationalized by introducing the relaxation of *d*-band holes as an effective excitation process for hot electrons. The lifetime of *d*-band holes can then be estimated from the difference in relaxation times observed for the distinct electron excitation pathways. A simulation of the hot electron transport out of the near-surface region, which is based on electron velocities derived from a band structure calculation, reproduces the trend of the crystal face dependence of the relaxation times, observed by Ogawa *et al.*[31] By quantifying the influence of the transport effect, electron lifetimes are deduced from the experimentally observed relaxation times and compared to *d*-band hole lifetimes at the same excess energy.

II. METHOD

In two-photon photoemission the photon energies ($h\nu$) do not exceed the substrate work function (Φ) to prevent the superposition of the spectra with electrons emitted by one-photon photoemission. Thus in 2PPE the photoemitted electrons yield information about the normally unoccupied intermediate states between the Fermi and vacuum levels regarding their energetic positions, dispersions, and lifetimes.[34,35] If no inelastic scattering process is involved, the initial- (E_i) and intermediate- ($E_{\rm int}$) state energies with respect to the Fermi level can be deduced from the kinetic energy of the emitted electrons ($E_{\rm kin}$) by $E_{\rm int}=E_{\rm kin}+\Phi-E_{\rm probe}$ and $E_i=E_{\rm kin}+\Phi-E_{\rm probe}-E_{\rm pump}$, respectively, where $E_{\rm pump}$ and $E_{\rm probe}$ are the photon energies of the pump and probe pulses. Time resolution is achieved by using two laser pulses which are delayed with respect to each other. In an autocorrelation setup the same photon energy *and* polarization is used for both pulses, and therefore the detected autocorrelation trace (2PPE intensity of a certain final-state energy interval vs delay time) is symmetric with respect to time zero (temporal overlap of the pulses). By using two different photon energies (the fundamental and its second harmonic as in some experiments presented here), the symmetry in time is broken. The cross-correlation trace thus recorded provides additional information like the maximum of the trace with respect to time zero.[29,36]

In 2PPE, the electrons can emitted via different excitation pathways. In the case of the occupied surface state on Cu(111), the 2PPE signal is caused by an instantaneous two-photon transition involving only virtual intermediate states, which results in a correlation trace given by the correlation function of the two laser pulses (temporal convolution of the pulse intensities). In most cases, however, an intermediate state is temporarily populated between the two steps of the excitation. Between these two excitation steps inelastic scattering (by electrons) or quasielastic scattering (by phonons, defects) may occur. On the other hand, the relaxation of the photogenerated electrons (and holes) leads to additional ''secondary'' electrons, which dominate the electron distribution at low-lying intermediate states ($E_{\rm int}<0.5$ eV for $E_{\rm pump}>\sim3.0$ eV).[11] The pure lifetime of an intermediate state can be directly observed only when inelastic scattering into this intermediate state (by secondary electrons) as well as the ballistic transport out of the detection volume does not occur. This requirement is fulfilled for discrete states localized at the surface, i.e., image potential states[14,37–39] and adsorbate-induced states.[40–42] In the case of the hot electrons, however, 2PPE reflects the electron population in (delocalized) bulk states in the *near-surface region*, which is defined by the skin depth. The time evolution of this hot electron distribution is the relevant quantity in a substrate-mediated photochemical process. The pure hot electron lifetimes, however, which should be compared with the theoretical values from Fermi liquid theory,[9,10] can only be deduced if the influence of ballistic transport and secondary-electron generation is known.

In the upper part of Fig. 2, the 2PPE spectrum of a clean Cu(111) surface at a photon energy of 4.75 eV is plotted versus the final-state energy. The spectrum is mainly characterized by three features: (i) At high final-state energies

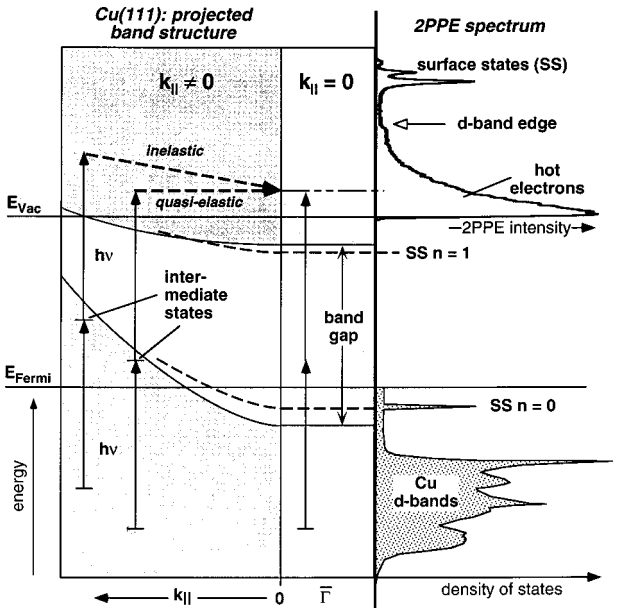

FIG. 2. 2PPE spectrum of Cu(111) at $h\nu = 4.75$ eV, density of initial states (DOS) of Cu, and projected band structure of Cu(111). In 2PPE spectrum features of the occupied ($n=0$) and unoccupied ($n=1$) surface states are observed at high energies. The drop in 2PPE intensity is due to the decrease in the DOS. Hot electrons with a nonvanishing lifetime in an intermediate state can only be excited at $k_\parallel \neq 0$.

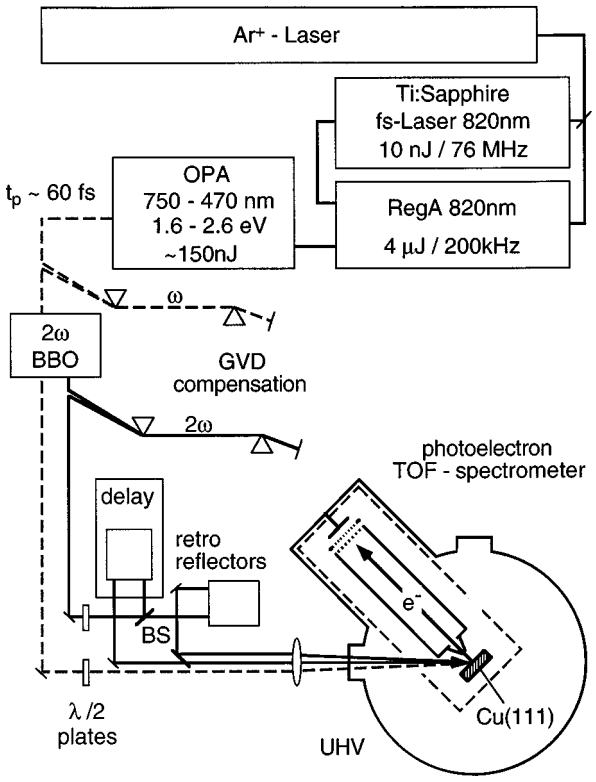

FIG. 3. Experimental setup.

three sharp peaks are observed, which arise from occupied and unoccupied surface states.[38] (ii) The sharp decrease of the density of initial states due to the *d*-band edge (see DOS in the lower part of Fig. 2) leads to a drop in the 2PPE intensity at the corresponding final-state energy. (iii) At low final-state energies, the 2PPE spectrum is dominated by hot (secondary) electrons. In order to elucidate the excitation pathway of these hot electrons, the projected band structure of Cu(111) is shown on the left side of Fig. 2.

In the experiment we detect the photoemitted electrons from the Cu(111) surface in the normal direction ($k_\parallel = 0$, $\bar{\Gamma}$ point). Thus instantaneous two-photon transitions via virtual states can occur at $k_\parallel = 0$ due to the *sp*-band gap, which extends from 0.85 eV below to 4.15 eV above the Fermi level.[35,36] As the hot electrons show relaxation times up to a few hundred femtoseconds, they obviously populate real intermediate states at $k_\parallel \neq 0$ and are scattered into the direction of the detector in the final state (see left side of Fig. 2). A quasielastic scattering process (*e*-ph, $\Delta E \approx 15$ meV;[7,8] *e* defect, $\Delta E \approx 0$ meV) conserves the information about the intermediate-state energy, while for an inelastic scattering process (*e*-*e*) this information is lost. The ratio between quasielastic and inelastic scattering processes is not known. However, we assume that due to the large phase space for inelastic scattering processes into lower-lying states below E_{vac} inelastic scattering into states above E_{vac} plays only a minor role (see Fig. 2). This view is supported by the observation of a relatively sharp *d*-band edge in the 2PPE spectra.

We can, therefore, conclude that on Cu(111) the 2PPE experiment samples the electron dynamics integrated over an extended part of the Brioullin zone rather than at a certain $k_\parallel$ vector. For two different crystal faces and for intermediate-state energies where no real intermediate states exist in the direction of detection (projected band gap), we would then expect that the 2PPE experiment samples in both cases the dynamics of electrons with *all* possible *k* vectors and should thus yield equal results. Experimentally, however, a pronounced difference between the relaxation times on the Cu(111) and Cu(100) surfaces was observed by Ogawa *et al.*[31] for $E_{\mathrm{int}} > 2$ eV, intermediate-state energies where both crystal faces possess a projected band gap.[43] The observed crystal face dependence can be partly explained when the influence of the ballistic transport on the effective relaxation times is included (see Sec. V C). The crystal face dependence arises then from differences in the electron velocity distribution projected onto the surface normal.

III. EXPERIMENTAL SETUP

In the experiment femtosecond laser pulses at 810 nm are generated by an Ar^+-laser (Coherent, Innova I-415) pumped Ti:sapphire oscillator (MIRA 900) and subsequently amplified to 4 μJ/pulse in a regenerative amplifier (RegA 9000) at a 200-kHz repetition rate (Fig. 3). The RegA output pumps an optical parametric amplifier (OPA 9400), in which a linearly chirped white light continuum is mixed with the frequency-doubled pulse (405 nm) in a β-barium borate (BBO) crystal of 1 mm thickness. The matching angle of the crystal as well as the time delay between the second harmonic and the white light pulse determine the spectral components amplified from the white light continuum.[44] After two amplification processes using the same crystal in a double-pass configuration, an OPA signal output power of 100 nJ/pulse is obtained. With a pair of SF10 prisms the tunable femtosecond pulses (470–730 nm) are compressed to a nearly Fourier-limited pulse of 50–80 fs [full width at half

maximum (FWHM)].[45] The pulse width of the OPA output is restricted by the amplified spectral bandwidth and therefore depends on the wavelength. The shortest pulses are obtained for low photon energies. By detuning the time delay between the white light and the second harmonic in the second pass, slightly different spectral components compared to the first pass are amplified, which results in a spectral broadening of the output pulse. In this manner the pulse width can be further reduced by 20% to 40 fs at 700 nm (70 fs at 500 nm) at the cost of about a third of the output power.

The compressed OPA output is focused into a 0.2-mm-thick BBO crystal (type I) by a 200-mm lens, generating the second harmonic. After separating the two beams by a dichroic mirror, the polarization of the UV beam is flipped to horizontal polarization and the UV pulse is compressed by another pair of quartz prisms. For autocorrelation measurements a broadband 1:1 beam splitter (BS) is used to split the UV pulse into two beams, of which one is delayed with respect to the other by a computer-controlled delay stage (1 step=0.05 fs). For recombination of the pulses a second beam splitter is used, so that each beam traverses the same amount of optical material (Mach-Zehnder setup; see Fig. 3). In this way the chirp added to both pulses is the same and can therefore be compensated by the quartz prisms. To avoid interferometric effects the beams are focused onto the sample noncollinearly (skew 0.5°) by a fused silica lens positioned outside the UHV chamber ($f=500$ mm). For the cross-correlation (two-color) setup, the beam splitters are replaced by mirrors and the entire UV beam (with variable delay) is used together with the fundamental of the OPA output (see Fig. 3).

The two beams enter the UHV chamber through a 1-mm-thick MgF_2 window and hit the sample at an angle of 45° with respect to the surface normal. For two-color 2PPE as well as for time-resolved experiments, both pulses have to overlap in time and space on the sample. The spatial overlap is achieved by aligning the two beams into a pinhole (150-μm orifice), which is positioned at the same light path distance from the focusing lens as the sample. A strong rise in the overall 2PPE intensity indicates the temporal overlap upon varying the time delay. The exact determination of pulse width and zero delay between the pulses is important, because they are critical parameters for the data analysis. In all experiments we used the time-resolved two-photon photoemission response from the occupied surface state on Cu(111) as a reference.[29] Herein the electrons are excited via virtual intermediate states, which do not have a real lifetime, and therefore the temporal 2PPE signal follows the correlation function of the laser pulses. Assuming the same pulse width for both pulses and sech^2-shaped pulses, we deduce the pulse width and zero delay from the surface-state correlation trace. The absorbed fluence on the surface is of the order of 30 μJ/cm^2, so that the rise of the electronic temperature ΔT_e is below 75 K and space charge effects can be neglected.

The Cu(111) sample is mounted in an UHV chamber with a base pressure of 2×10^{-10} mbar between a pair of tantalum wires, which are in thermal contact to a copper mount attached to a He cryostat.[46] The crystal can be heated either resistively or by electron bombardment. By cooling with liquid helium a sample temperature of 20 K can be achieved. The Cu(111) crystal was cleaned by cycles of 10-min Ar^+ bombardment (700 eV) followed by 15 min of annealing at a temperature of 800 K. A sharp, low-background low-energy electron diffraction (LEED) pattern and a narrow linewidth of the surface state in the 2PPE spectrum served as criteria for the surface quality of the Cu(111) crystal. The sample was exposed to xenon through a pinhole doser with a 10-μm orifice.

All correlation experiments reported here were performed on a xenon-covered Cu(111) surface. Upon adsorption of a monolayer of xenon the work function is lowered by 0.5 eV to about 4.3 eV.[38] Therefore, the photon energy can be lowered accordingly, which allows us to generate shorter laser pulses and thus enhances the time resolution. It was verified that the electron dynamics in the energy range investigated in this paper does not change upon xenon adsorption. To optimize the preparation of a saturated monolayer of xenon on Cu(111), thermal desorption spectroscopy (TDS) was used.

The photoemitted electrons are detected in a time-of-flight (TOF) spectrometer, which is shielded electrically and magnetically by a cylindrical Co-Netic tube of 1.3 mm thickness. The electrons traverse a 3–4-mm-long distance from the sample before entering the graphite-coated time-of-flight tube through a 1.5-mm large opening at the tip of a cone. After drifting through the 30-cm-long field-free region, the electrons are accelerated onto a pair of multichannel plates. The angle of acceptance was estimated to be $\pm3.5°$ from the spectrometer axis. Using the white light leakage of the OPA measured by a fast photodiode as a time reference, the electron flight time is converted by a time-to-amplitude converter (TAC) and recorded by a triggered 100-kHz A/D converter (National Instruments, MIO-16H). The correlation traces of all energy intervals were detected simultaneously, thus excluding the influence of long-term laser drifts and changes in surface quality. Compared to an earlier setup,[46] the energy resolution of the spectrometer was improved to 15 meV (FWHM) at 1 eV kinetic energy.

IV. RESULTS

A. Correlation traces and analysis model

A correlation trace is obtained by recording the 2PPE signal of a certain final-state energy (E_{fin}) interval (typical width 100 meV) as a function of the time delay. Neglecting scattering events in the final state, the intermediate-state energy (E_{int}) can be calculated from the final-state energy as described earlier. In the upper plot of Fig. 4, the autocorrelation trace of an corresponding intermediate-state energy $E_{\mathrm{int}}=0.23$ eV is shown (dots). A photon energy of 4.2 eV was used, and the laser pulse width was 77 fs; as in all experiments described here, the laser light was polarized parallel to the plane of incidence (p-pol). In an autocorrelation experiment, the observed traces are symmetric with respect to zero delay, since pump and probe pulses cannot be distinguished. The autocorrelation trace in the upper plot of Fig. 4 shows a sharp peak around zero delay and long wings extending to a delay time of more than ±1 ps.

This particular shape of the autocorrelation trace has already been discussed in the literature,[31,40,47] it is composed of a fast component (dotted line, autocorrelation function of the laser pulses) and a slow component (dashed line). The

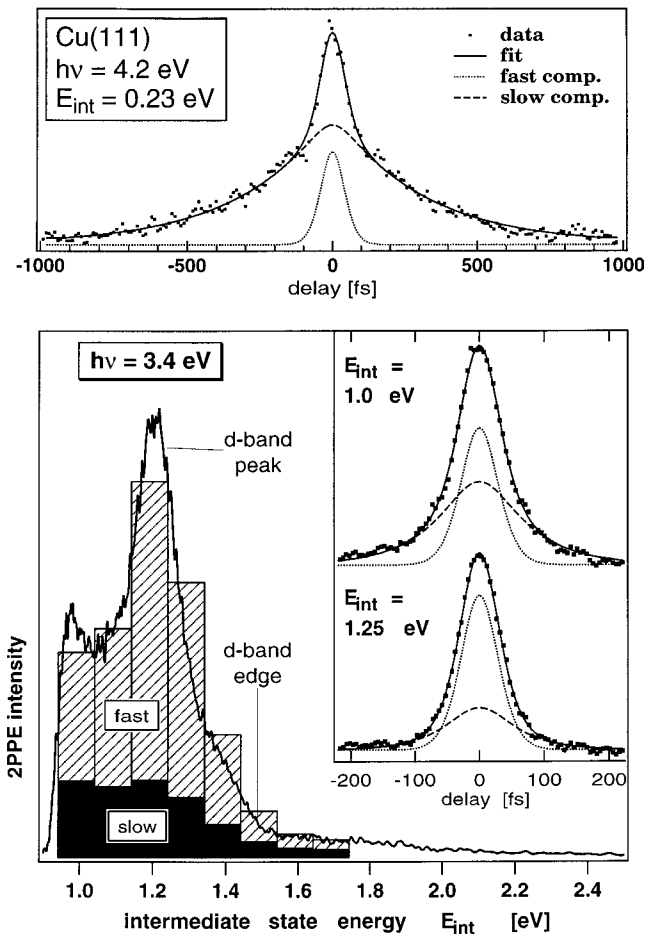

FIG. 4. A two-component fit model is used to fit autocorrelation traces (upper plot). The sharp d-band peak in a 2PPE spectrum (lower plot) arises from instantaneous two-photon transitions from the highest d bands at the L point, as can be deduced from time-resolved experiments (see text). The correlation trace follows then a correlation function of the laser pulses and therefore contributes only to the fast component in the fit. Inset: In the autocorrelation trace the fast component at $E_{\mathrm{int}}=1.25$ eV is stronger (79%) than at $E_{\mathrm{int}}=1.0$ eV (63%).

fast component is mainly due to the so-called coherent artifact, an enhancement, which is due to the fact that the electrical fields of both pulses add coherently and the energy of both fields is transferred to the electron in both excitation steps. The slow component reflects the electron dynamics in the intermediate state and is fitted with a convolution of the two laser pulses with an exponentially decaying function, where the decay constant is identified with the relaxation rate of the hot electrons. If the excitation pathway can be described by a two-step process via a real intermediate state, the ratio of the fast component, the slow component, and the constant background (sum of the 2PPE intensity of each individual pulse) is 1:1:1 for zero delay. However, electrons which are excited via instantaneous two-photon transitions would enhance the fast component, while secondary electrons generated by an inelastic scattering process would enhance the slow component. For these reasons (and in contrast to other approaches[31]), the amplitude ratio between the fast and slow components was used as a free parameter, together with the absolute amplitude of the autocorrelation signal, an additive constant for the background, and the relaxation time τ_r in the intermediate state.

The amplitude ratio of the fit can also be used to identify the excitation pathway of distinct structures in the spectra. At a low photon energy (3.4 eV), a sharp peak at about 250 meV below the d-band edge ($E_{\mathrm{int}}=1.25$ eV) is observed (see lower part of Fig. 4); its photon energy dependence identifies it as an occupied state. The correlation trace at $E_{\mathrm{int}}=1.25$ eV yields a fast-to-slow amplitude ratio of 3.7:1, compared to an amplitude ratio of 1.7:1 at $E_{\mathrm{int}}=1.0$ eV (see inset). As only the contribution of the fast component to the 2PPE intensity (hatched area) rises in the d-band peak, we can conclude that this feature arises from instantaneous two-photon transitions. This effect was also observed in a cross-correlation experiment, where at low intermediate-state energies the instantaneous two-photon transitions from the d-band contribute significantly to the fast component of the correlation trace (not shown). By comparing the initial-state energy ($E-E_{\mathrm{Fermi}}=-2.25$ eV) with the calculated band structure of Cu, the d-band peak can be assigned to transitions from the energetically highest d bands at the L point (L_{4^+},L_{5^+},L_{6^+}).[43] Due to the existence of a projected band gap on Cu(111), instantaneous two-photon transitions play a more important role as on the other crystal faces.

For a cross-correlation setup, there is no coherent artifact. However, an additional excitation pathway contributes to the signal, where the UV pulse acts as the pump pulse and the visible pulse serves as the probe pulse. In a cross-correlation setup, the symmetry in time is broken, and thus the relaxation dynamics arising from one or the other excitation pathway (UV pump or visible pump) can at least in principle be distinguished in a time-resolved experiment. Moreover, if the UV pulse acts as the pump pulse, the hot electron lifetimes are believed to be relatively short lived (10–20 fs) (Refs. 30–32) due to the high intermediate-state energy ($E_{\mathrm{int}}>2.5$ eV). Therefore, the relaxation dynamics for this process can be described by a fast fit component in a first approximation. In contrast to an earlier publication,[29] we used a similar two-component fit model for the cross-correlation experiment as for the autocorrelation experiment in order to account for this second excitation pathway and for instantaneous two-photon transitions (results are shown in Fig. 5).

B. Relaxation times

In the upper part of Fig. 5, various relaxation time traces derived from cross-correlation ($h\nu=2.2$ eV) and autocorrelation experiments ($h\nu=3.4$, 3.6, 3.81, and 4.2 eV) as well as the hot electron lifetimes calculated from Fermi liquid theory are shown as a function of the intermediate-state energy E_{int}. Note the semilogarithmic scale. For $E_{\mathrm{int}}<1.1$ eV the relaxation times for all photon energies decrease with increasing E_{int} and agree well within the experimental error. The relaxation times obtained from the cross-correlation experiment deviate slightly (especially for higher E_{int}) from previously published data.[29] This might be due to the improved fit model (with two components) used in this analysis. For higher E_{int} (1.3–1.8 eV), the relaxation times increase again and show a strong dependence on photon

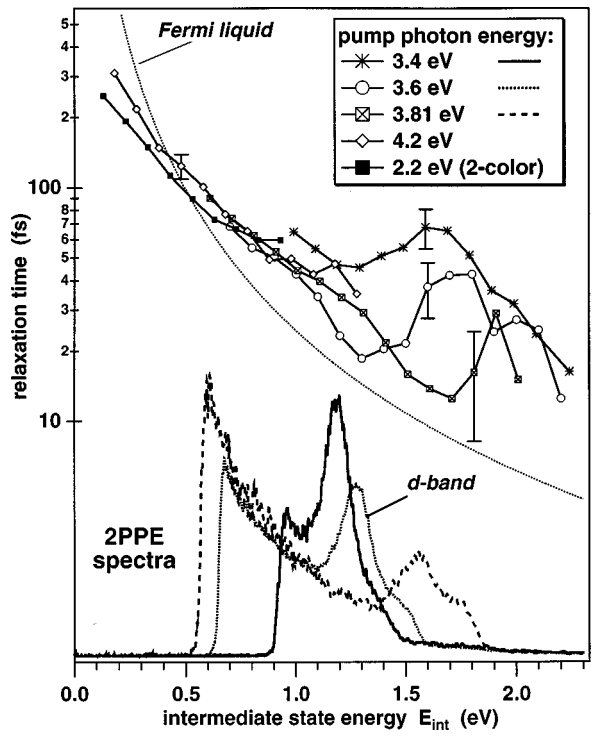

FIG. 5. Relaxation times derived from auto- and cross-correlation experiments for five different pump photon energies plotted vs the intermediate-state energy (upper part). Corresponding 2PPE spectra for $h\nu=3.4$, 3.6, and 3.81 eV (lower part).

energy. At $E_{\text{int}}=1.65$ eV the values obtained for the relaxation time vary from 13 ± 4 fs at $h\nu=3.81$ eV to 67 ± 10 fs at $h\nu=3.4$ eV. In order to discuss this apparent dependence of the lifetime on photon energy, the corresponding 2PPE spectra are shown for three photon energies (3.4, 3.6, and 3.81 eV) in the lower part of Fig. 5. In all spectra a peak due to the d band is observed, which is followed by a sharp drop in 2PPE intensity at higher energies due to the d-band edge (see DOS in Fig. 2). The relaxation time minima coincide with the d-band peaks, while the relaxation time maxima are located just beyond the d-band edge, where electrons can no longer be excited from the d bands.

This unusual correlation of relaxation times with band structure was observed on a Cs-covered Cu(111) surface by Pawlik *et al.*[33] The authors interpreted the pronounced minimum of the relaxation time at the position of the d-band peak as a minimum in the lifetimes of the sp-band electrons and assigned it to a fast decay channel, which is only present if electrons are excited *directly* from the d band.[30] It was proposed that the electrons excited to the sp band in a vertical transition preferentially recombine with their own d-band holes on a short time scale. However, we would argue that this proposed process should also occur for any transitions from a d band to the sp band and not only for electrons at the d-band peak. Furthermore, the energy from the electron-hole recombination process leads to the generation of another electron-hole pair, which is most likely a hole in the d bands and an electron in the sp band due to the high DOS of the d band. Thus the hot electron distribution should only be insignificantly altered by this proposed recombination process. Cao *et al.*[32] also observed a similar dependence of the relaxation times on the intermediate-state energies on a Cs-covered Cu(100) surface and for a K-covered polycrystalline copper film. The authors proposed that the pronounced rise and the maximum of τ_r above the d-band edge might be attributed to the existence of longer-lived excitonic states consisting of excited d-band electrons and their holes. It was argued that the localization of the excited electron at the hole reduces the scattering probability and thus leads to an increase in the lifetime. However, even if excitonic states would exist in metals (which seems rather unlikely due to the efficient screening in metals), the experimental results contradict this scenario: (i) At the intermediate-state energies where the longer relaxation times are observed (i.e., above the d-band edge), electrons *cannot* be excited from the d bands; (ii) however, at the intermediate-state energies where direct excitation from the d band is possible (and thus longer relaxation times would be expected), a pronounced *minimum* in the relaxation time is observed. Therefore, we do not follow the interpretations given by Pawlik *et al.*[30,33] and Cao *et al.*[32] and will discuss in the following an alternative excitation mechanism (mentioned by Aeschlimann[48]), which accounts for the observed dependence of τ_r on the photon energy, especially for the longer relaxation times above the d-band edge.

V. DISCUSSION

The most striking result of the correlation experiments is the dependence of the relaxation times on the band structure, which results in longer relaxation times at intermediate-state energies where the electrons can no longer be excited from the Cu d bands. In the first part of this section, we will discuss this apparently longer lifetime by looking at the excitation mechanisms of these electrons in more detail. An estimation of the lifetime of a d-band hole is given in the second part, while in the third part simulations of the influence of ballistic electron transport on the dynamics of photogenerated hot electrons probed by 2PPE are presented.

A. Auger excitation via d-band hole decay

Photoabsorption of the pump pulse in a metal results in the generation of electron-hole pairs within the penetration depth of the light (~150 Å). In copper, the excitation of a d-band electron to the unoccupied part of the sp band is the dominant absorption process for $h\nu>2$ eV, due to the higher probability of direct transitions compared to indirect excitation and to the high density of d-band states (see Fig. 2). This fact is reflected in the optical properties of copper, which shows a sharp decrease in reflectivity above a photon energy of 2 eV.[49] As the Cu(111) surface has a gap in the projected band structure, the first excitation step must take place at points in k space with nonvanishing parallel momentum (see Fig. 2). We will discuss the different excitation mechanisms using the band structure along the $\langle110\rangle$ direction as schematically shown in Fig. 6.[43]

The direct transition from the d band to an unoccupied state in the sp band is denoted as process A. By this process electrons can only be excited up to a certain intermediate-state energy (in this example, for $h\nu=3.6$ eV, the threshold is at an intermediate-state energy of $E_{\text{thres}}=1.6$ eV). This leads to a drastic drop in the 2PPE intensity at higher ener-

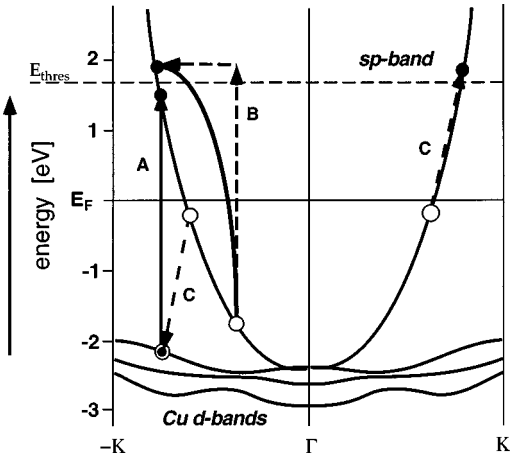

FIG. 6. Electron excitation mechanisms: (A) direct excitation from a d band to the sp band, (B) indirect intraband transition, and (C) Auger excitation: generation of a d-band hole by direct transitions followed by an Auger decay of a d-band hole.

gies (see Fig. 5). However, electrons can also be excited above E_{thres} by an indirect sp-interband transition (process B). In this case the electron must scatter with a defect or a phonon in order to conserve momentum. Due to the low density of initial sp-band states (Fig. 2) and the requirement of an additional scattering process, these transitions are much less likely than direct transitions (A). However, the decay of photogenerated d-band holes also results in the generation of hot (secondary) electrons (process C). Due to the high probability of direct transitions (A), d-band holes are generated in large number. The relaxation of these d-band holes can be viewed as an Auger process, where one electron fills the hole and transfers the excess energy to another electron, which is excited above the Fermi level (C). The intermediate-state energy of this electron can be as high as the energy of the hole with respect to the Fermi level and can thus reach at maximum the photon energy.

The generation rate of hot electrons excited via intraband or interband transitions (processes A and B) follows the intensity of the pump pulse. For process C the generation of the d-band *holes* also follows the intensity of the pump pulse, but the *electron* population excited through Auger decay builds up at later times, namely, with the decay of the d-band holes. Assuming an excitation via Auger decay, the longer relaxation times at intermediate-state energies above the d-band edge ($E_{\text{int}} > E_{\text{thres}}$; see Fig. 5) can now be rationalized, since the observed electron dynamics includes an additional contribution of the d-band hole lifetime. It is most likely that this Auger-type excitation mechanism (C) is more efficient than the competing indirect transition (B) due to effective generation of d-band holes in the primary absorption step and due to the momentum-conserving excitation of the Auger process. At lower intermediate-state energies ($E_{\text{int}} < E_{\text{thres}}$), the excitation process C is also present, but the 2PPE spectrum and the observed relaxation times are dominated by process A.

An additional experimental indication for the effective excitation of electrons via a hole decay was given Perner *et al.*[50] The authors investigated the optically induced damping of the surface plasmon resonance in gold colloids (d-band edge, $E_{\text{thres}} = 2.3$ eV). It was found that the damping rate follows the scattering rate of the photogenerated electrons. In their calculation the authors had to include a similar hot electron generation process via d-band holes in order to describe the experimental findings correctly.

To further test the effectiveness of the Auger excitation process, we also performed cross-correlation experiments on bare Cu(111) by varying the photon energy of the pump pulse, but leaving the probe pulse energy unchanged. For a pump pulse energy above 2 eV, a high intensity of the cross-correlation signal with respect to the background was observed even at intermediate-state energies where electrons cannot be excited directly from the d band. This strong signal was assigned to electrons originally excited by d-band hole decay. Upon lowering the photon energy below 2 eV, no d-band holes could be generated and the cross-correlation signal with respect to the background dropped sharply.

In this framework the observed longer relaxation times on gold[28] (d-band edge, -2.3 eV, comparable to copper) can also be explained when assuming an Auger excitation process, while the relaxation dynamics on silver (d-band edge, -4 eV) occurs on a much faster time scale if the pump pulse energy is lower than 4 eV (see Aeschlimann *et al.*,[28,48] $h\nu = 3.3$ eV).

B. Lifetimes of d-band holes

From the differences in relaxation times observed for electrons excited via direct transitions (process A in Fig. 6) compared to those excited via Auger decay (C), it should be possible to estimate the lifetime of a d-band hole. At an intermediate-state energy of $E_{\text{int}} = 1.65$ eV, the observed electron relaxation time is 13 ± 4 fs for $h\nu = 3.81$ eV (process A), while for $h\nu = 3.4$ and 3.6 eV (process C) relaxation times of 67 ± 10 and 42 ± 8 fs, respectively, were measured for the same intermediate-state energy (see Fig. 5). On the basis of a three-level rate equation model, we present a simulation of the *delayed* electron excitation by a d-band hole decay in order to quantify the influence of this excitation mechanism on the observed electron relaxation times. In the first step d-band holes are generated via direct transitions from the d band to the sp band (see inset of Fig. 7). The generation rate of the d-band holes (R_h) is given by the intensity of the pump pulse, which was assumed to be of the form $\text{sech}^2(at)$ (pulse width, 50 fs). The decay of these photoexcited holes leads then to the excitation of electrons into an intermediate state. For simplicity we assume a single lifetime for all d-band holes (in the simulation shown in Fig. 7, $\tau_h = 35$ fs). The rate of the electron excitation (R_e) is then given by

$$R_e(t) \propto \int R_h(t') \exp\left(\frac{t-t'}{\tau_h}\right) \theta(t-t')\, dt', \qquad (1)$$

with the step function $\theta(t)$, which is defined by $\theta(t) = 0$ for $t < 0$ and $\theta(t) = 1$ for $t \geq 0$. The excited electron population is assumed to decay with a relaxation time of $\tau_r = 15$ fs. As the electron relaxation dynamics itself remains unaffected by the excitation process, we will not consider the influence of the transport effect here (see Sec. V C). For the d-band holes the ballistic transport is negligible on this time scale, and secondary electrons only play a minor role at this high

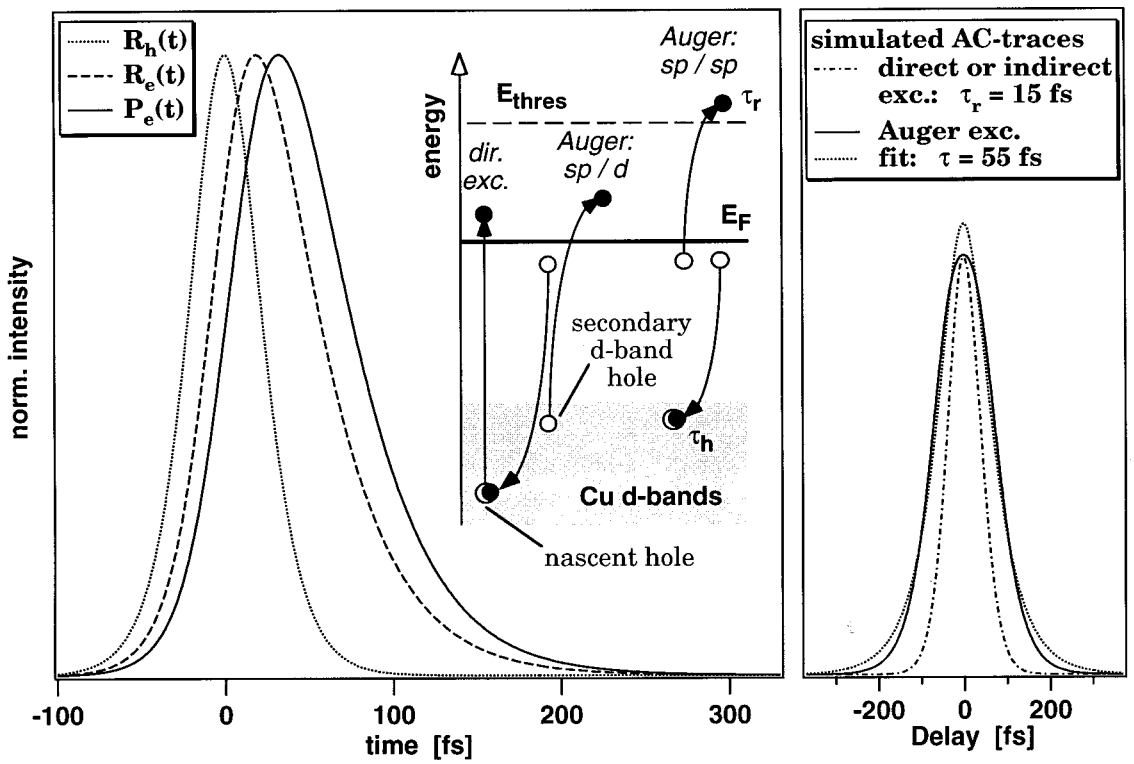

FIG. 7. Left: simulated generation rate of d-band holes (R_h) and electrons (R_e) and electron population (P_e) assuming a laser pulse width of 50 fs, a hole lifetime of $\tau_h = 35$ fs, and an electron relaxation time of $\tau_r = 15$ fs. Right: the fit to the simulated autocorrelation trace yielding an effective relaxation time of $\tau = 55$ fs. Inset: A d-band hole can decay via different channels depending on the origin of the involved electrons. Decaying holes generate secondary holes in the upper d bands, if a d-band electron is involved in the Auger process.

intermediate-state energy. From the electron excitation rate and the electron relaxation time, the electron population in the intermediate state (P_e) can be deduced as

$$P_e(t) \propto \int R_e(t') \exp\left(\frac{t-t'}{\tau_r}\right) \theta(t-t') dt'. \qquad (2)$$

In the left graph of Fig. 7, the generation rates of the holes and electrons as well as the electron population are plotted versus time. Due to the delayed excitation process, the maximum of the electron population (P_e) is only reached when the pump pulse intensity has almost dropped to zero. The convolution of the electron population with the probe pulse (50 fs, sech^2 shape) leads to a cross-correlation trace, from which the autocorrelation trace (solid line in the right plot of Fig. 7) is derived by symmetrization in time. The fitting procedure outlined above, with the amplitude ratio of fast-to-slow components set to zero, yields a relaxation time of 55 fs (dotted line), which is on the order of the experimentally observed relaxation times (67 fs for 3.4 eV, 42 fs for 3.6 eV). For comparison, the simulated autocorrelation trace assuming direct (or indirect) electron excitation is also shown in the figure (dash-dotted line). By varying electron relaxation times and hole lifetimes in the simulation, it can be concluded that to a first approximation the observed relaxation times for Auger-excited electrons are increased by approximately the hole lifetime compared to electrons excited via direct or indirect transitions. However, for longer hole lifetimes or relaxation times ($\tau_h + \tau_r > 55$ fs), the fit no longer reproduces the simulated autocorrelation traces correctly.

Since d-band holes are generated in a wide energy range ($-h\nu < E - E_{\mathrm{Fermi}} < -2$ eV), the assumption of a single lifetime for all d-band holes is a strong simplification, because the phase space for hole scattering (Auger excitation) and thus the lifetime vary with energy. The d-band hole lifetime is expected to be longest for holes at the d-band edge ($E - E_{\mathrm{Fermi}} = -2$ eV). This view is supported by the experimental results of Matzdorf *et al.*,[51] who derived *lower* limits for the d-band hole lifetime in copper in an energy range of -3.7 eV$\leqslant E \leqslant -2$ eV by using linewidth analysis in high-resolution angle-resolved photoemission. It was found that the linewidth decreases almost linearly from 180 meV at $E - E_{\mathrm{Fermi}} = -3.7$ eV to 60 meV at $E - E_{\mathrm{Fermi}} = -2$ eV, which corresponds to a lower limit for the hole lifetime of 10 fs (at $E - E_{\mathrm{Fermi}} = -2$ eV).

Photogenerated holes in lower-lying d bands can be filled either by sp-band electrons or by electrons from higher d bands (see inset in Fig. 7). On the other hand, the electron excited above the Fermi level in an Auger process can originate either from a d band or from the sp band. Due to the higher density of states of the d bands compared to the sp band (see Fig. 2) and due to considerations of momentum conservation, it is most likely that in the Auger decay of a hole in a lower-lying d band one sp-band electron and one d-band electron are involved (Auger: sp/d in Fig. 7). Thereby, the excess energy of the excited electron cannot exceed E_{thres}, which corresponds to the d-band edge in the 2PPE spectrum. On the other hand, this process leads to the generation of a *secondary hole* in an upper d band. For excitation above E_{thres}, two sp-band electrons must be in-

volved (Auger: sp/sp in Fig. 7), a process which is the only decay channel for holes as the upper d band edge. This suggests that the d-band holes cascade towards the upper edge of the d bands at -2 eV via Auger processes involving d-band electrons, before they decay via Auger processes involving two sp-band electrons.

In this scenario, however, most of the Auger electrons will be excited to an intermediate state with an energy of $E_{\mathrm{int}}\sim 2$ eV at maximum. Interestingly, the experimentally observed relaxation rates on all three low-index copper surfaces seem to drop sharply at an intermediate-state energy of $E_{\mathrm{int}}\sim 2$ eV (see Fig. 5 and also Pawlik *et al.*[30] and Ogawa *et al.*[31]), above which Auger excitation might only play a minor role. Following the above argumentation, the d-band hole lifetime used in our simulation can therefore be interpreted as a relaxation time for a hole in an upper d band for an Auger decay via two sp-band electrons. This relaxation time is then approximately the lifetime of a d-band hole at $E-E_{\mathrm{Fermi}}=-2$ eV, since Auger decay via two sp-band electrons is the only relaxation channel for these holes.

In the following we try to compare the d-band hole lifetime of 35 fs found in our simulation with the lifetimes of electrons in the sp band for the same excess energy. In comparison to the theoretically derived electron lifetime of 6 fs from Fermi liquid theory at $E-E_{\mathrm{Fermi}}=2$ eV, the d-band hole lifetime is substantially longer. But as pointed out by Ogawa *et al.*,[31] Fermi liquid theory underestimates the efficient screening in metals, which reduces the scattering probability and thus enhances the lifetime. A comparison of the hole lifetime with the observed electron relaxation times, however, is not very conclusive, since the relaxation times (even if excited by direct transitions) do not represent the electron lifetimes, because the observed relaxation dynamics is further influenced by the ballistic electron transport out of the detection volume. In order to quantify the transport effect and finally to extract electron lifetimes, we have carried out simulations on the basis of a band structure calculation, which will be presented in the next section.

C. Transport effect

The penetration depth of UV light at 3.5 eV photon energy is about 150 Å, while the probe depth is only 30 Å according to the universal curve of the electron mean-free-path length (see Fig. 8).[52] In copper electrons at the Fermi level have a velocity of the order of 10^8 cm/s (15 Å/fs).[53] According to their velocity perpendicular to the surface ($v_\perp$), a large number of photoexcited electrons move within a few tens of femtoseconds after excitation from the surface into the bulk, where they cannot be probed by the second pulse (see Fig. 8). The reduction of the hot electrons within the probe depth caused by the electron motion is called the transport effect. This effect was already mentioned by Schmuttenmaer *et al.*[27] and investigated by Aeschlimann *et al.*[28] on polycrystalline gold films of variable thickness. Numerical calculations showed that the hot electron population in the near-surface region is drastically reduced in the first 30 fs.[11,28] Here we present simulations where we also include the anisotropy of the electron velocities and thereby derive a velocity distribution in the direction normal to the surface, which depends on the crystal face.

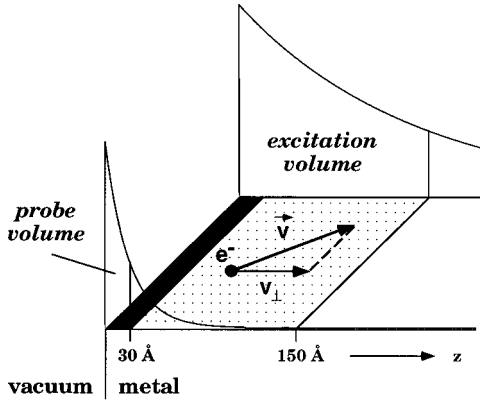

FIG. 8. Sketch of the penetration depth of the pump pulse (150 Å) and of the probe depth (30 Å). According to their projected velocity ($v_\perp=0-15$ Å/fs), some photoexcited electrons leave the near-surface region (transport effect).

1. Velocity distributions

For the ballistic transport of electrons at a certain intermediate-state energy, only the velocity distribution perpendicular to surface $D(v_\perp)$ is of relevance. Therefore, we have first to calculate the electron velocities $\vec{v}(\vec{k})$, which are given by

$$\vec{v}(\vec{k})=\frac{1}{\hbar}\nabla_{\vec{k}}E(\vec{k}), \tag{3}$$

where $E(\vec{k})$ is the band structure of the (unoccupied) Cu sp band. The constant-energy surfaces and the corresponding velocities were calculated for four intermediate-state energies $E=E_{\mathrm{Fermi}}$, 1.5, 2.5, and 3 eV using the empirical pseudopotential method[54,55] with the pseudopotential parameters of Fong *et al.*;[56] the Fermi level was set to $E=8.75$ eV. Despite the good agreement of the calculated band structure with the literature,[43,57] the $\vec{k}$-dependent velocities at $E=E_{\mathrm{Fermi}}$ are by $\sim 15\%$ higher than the experimentally observed Fermi velocities using the de Haas–van Alphen method.[53] However, the agreement with the theoretical results from Lee[58] is satisfactory.

To obtain the velocity distribution for an energy interval $[E,E+dE]$, the velocities were integrated over the respective constant-energy surfaces with a weighting factor of $|\nabla_{\vec{k}}E(\vec{k})|^{-1}\sim|\vec{v}(\vec{k})|^{-1}$. For each low-index copper surface, these velocity distributions were then projected onto the surface normal (see Fig. 8) to obtain the velocity distributions perpendicular to the surface $D(v_\perp)$, which are the relevant quantities for a comparison with the experiment. In Fig. 9 the velocity distributions $D(v_\perp)$ at $E_{\mathrm{int}}=1.5$ eV for the $\langle 100\rangle$, $\langle 110\rangle$, and $\langle 111\rangle$ crystal faces are shown. The velocity distribution for a free electron gas is constant up to the maximum velocity of 17.4 Å/fs at this intermediate-state energy. In contrast to this, the velocity distributions from the Cu band structure show sharp features, which arise at different velocities $v_\perp$ for different crystal faces due to the projection process.

2. Depletion of the electron population at the surface

Using the velocity distribution discussed above, we simulated the decrease of the hot electron population in the probe

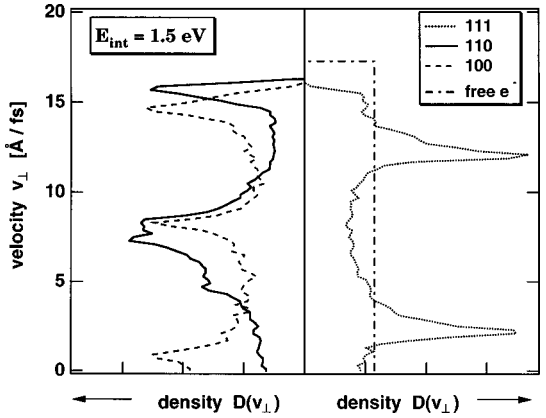

FIG. 9. Velocity distributions perpendicular to the surface $D(v_\perp)$ for the three low-index copper surfaces and a free electron gas at $E_{\rm int}=1.5$ eV.

volume, which will be described in the following. At this point, our simulation describes only the decrease of the electron population due to the pure ballistic transport; the decay of excited electrons was not included. The velocity distribution $D(v_\perp)$ is multiplied with an exponentially decaying spatial function according to a skin depth of 150 Å (see also Fig. 8). At each time step (1 fs), the electrons move according to their perpendicular velocities, thus creating a new space-dependent velocity distribution. It was assumed that electrons which reach the surface are elastically reflected back into the bulk. At the left side of Fig. 10, the velocity distribution for $E_{\rm int}=1.5$ eV is plotted at three simulation times for $z=50$ Å. For $t=0$ fs the velocity distribution is symmetric with respect to the movement either towards the surface or into the bulk. At later times most of the fast electrons already disappeared into bulk. The velocity distribution is now asymmetric; more electrons move into the bulk than towards the surface. For $t=60$ fs only electrons with small $v_\perp$ values remain in the detection volume.

At each time step the electron population in the near-surface region, which corresponds to an experimentally observable 2PPE intensity, can be simulated by weighting the space-dependent velocity distribution according to the effective probe depth (30 Å electron free mean path) and finally integrating over space and all velocities. The resulting depletion traces are shown for the three low-index surfaces and for the free electron gas on the right side of Fig. 10 for $E_{\rm int}=1.5$ eV. Half of the population is swept out of the probe volume within the first 20 fs: at longer times the depletion is slower and shows a crystal face dependence.

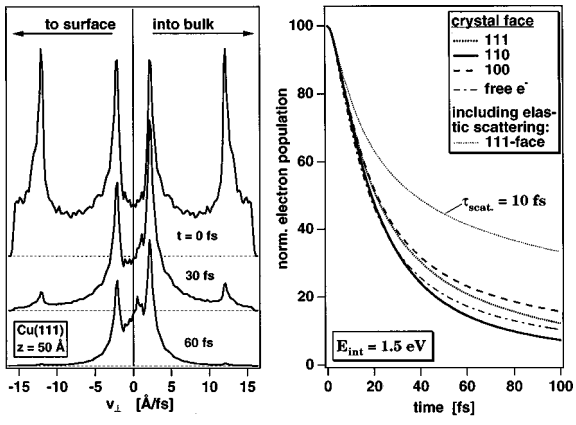

FIG. 10. Left panel: velocity distribution $D(v_\perp)$ for Cu(111), $E_{\rm int}=1.5$ eV at $z=50$ Å for three simulation times (0, 30, and 60 fs). Right panel: half of the electron population in the near-surface region (30 Å) removed within the first 20 fs. Especially for longer times the hot electron population depends on the crystal face. Elastic scattering processes reduce the transport effect (dotted weak line; scattering time, 10 fs).

This crystal face dependence can be rationalized by the shape of the velocity distribution $D(v_\perp)$ in Fig. 9. As discussed above, only electrons with small $v_\perp$ values contribute to the hot electron population at longer times. Figure 9 shows that the number of electrons with small $v_\perp$ values ($v_\perp<3$ Å/fs) is lower for the $\langle 110\rangle$ face and larger for the $\langle 100\rangle$ face. Accordingly, the reduction of the electron population is fastest for the $\langle 110\rangle$ face and slowest for the $\langle 100\rangle$ face (see Fig. 10). The electron population decrease for a free electron gas lies between the traces for the $\langle 110\rangle$ and $\langle 111\rangle$ surfaces.

At $E_{\rm int}=2.5$ eV, however, the electron population for the $\langle 100\rangle$ surface decreases slightly faster than for the $\langle 111\rangle$ surface, and this trend is even more pronounced at $E_{\rm int}=3.0$ eV (not shown). This can be rationalized by the opening of a new band gap in the $\langle 100\rangle$ direction for $E_{\rm int}>2$ eV, because the number of electrons with small $v_\perp$ values is then reduced. The $\langle 100\rangle$ face is therefore the only crystal face for which the transport effect increases with increasing intermediate-state energy. For the other surfaces only a weak dependence on intermediate-state energy is found in our simulation. For a free electron gas, however, the transport effect always increases for increasing intermediate-state energy (increasing maximal velocity $v_\perp$).

The above simulation accounts only for the pure ballistic transport; neither elastic nor inelastic scattering processes have been included. Elastic scattering processes with phonons and defects, however, can compensate the effect of ballistic transport to a certain extent (see also Knoesel *et al.*[11]). Hereby, the transport becomes diffusive and electrons moving into the bulk may actually reverse their direction and reenter the detection volume. As an example, we have assumed a mean elastic scattering time of $\tau_{\rm scat}=10$ fs. For the $\langle 111\rangle$ crystal face, the hot electron population decreases to 50% then in 38 fs compared to 21 fs without elastic scattering (see dotted lines in right graph of Fig. 10). This redistribution of momentum through elastic scattering on a relatively short time scale also smoothens the crystal face dependence of the effective electron population.

3. Comparison with experimental results

In the following the influence of the pure ballistic transport on the observed relaxation dynamics, i.e., the effect on the shape of the autocorrelation traces, will be discussed. Under certain conditions (high intermediate-state energy,direct excitation from the *d* band), the experimentally derived relaxation times are not influenced by secondary electrons, but certainly are affected by the ballistic transport. If the decrease of the electron population caused by the ballistic transport could be described by a single-exponential decay (i.e., by a transport relaxation time $\tau_{\rm trans}$), the hot electron lifetimes ($\tau_{\rm life}$) could be derived from the observed relaxation times (τ_r) using Matthiessen's rule (addition of inde-

pendent relaxation rates).[28] We deduce an effective τ_{trans} by folding the depletion traces with the pump and probe pulses and applying the two-component fit described in Sec. IV A. From the analysis of the simulated autocorrelation traces using various sets of parameters (pulse width, intermediate-state energy, lifetime), we can conclude that Mathiessen's rule ($1/\tau_r = 1/\tau_{life} + 1/\tau_{trans}$) can be applied for electron lifetimes from 20 to 80 fs within an error of only $\pm 5\%$.[59] The transport relaxation times (τ_{trans}) are found to be 67 fs for the $\langle 100 \rangle$ and $\langle 111 \rangle$ faces and 48 fs for the $\langle 110 \rangle$ face for a pulse width of 50 fs. These transport relaxation times are practically independent of intermediate-state energy (1.5–3.5 eV); only for the $\langle 100 \rangle$ face does the time increase by 15% for $E_{int} < 2$ eV.

According to Mathiessen's rule, the influence of the transport effect is small for short relaxation times ($\tau_r \ll \tau_{trans}$). For a high intermediate-state energy ($E_{int} = 1.65$ eV), where secondary electrons play only a minor role, and for direct electron excitation ($h\nu = 3.81$ eV), we deduce an electron lifetime of $\tau_{life} = 16$ fs from a relaxation time of $\tau_r = 13$ fs (see Fig. 5). This electron lifetime at $E_{int} = 1.65$ eV is shorter by more than a factor of 2 than the lifetime of a d-band hole at $E - E_{Fermi} = -2$ eV (see Sec. V B). As the electron lifetimes decrease with increasing intermediate-state energy, this lifetime difference is even higher at $E_{int} = 2$ eV. To a first approach, we would expect that the lifetimes of the hole and electron should approximately be the same due to the practically constant density of states in the sp band above and below the Fermi level. However,the necessity of momentum conservation might lead to a larger phase space for electron scattering than for Auger decay of the hole. The longer lifetime of the hole might also be partially rationalized by the fact that the d-band holes are localized, while the electrons in the sp band have a mean velocity of ~ 15 Å/fs. Following the argumentation of Cao *et al.*,[32] a localization might diminish the probability of scattering events and therefore enhance the lifetime.

For long electron lifetimes ($\tau_{life} > 100$ fs), the relaxation times would, according to Mathiessen's rule, approach the transport relaxation time. Since in the experiment (especially for $E_{int} < 0.6$ eV; see Fig. 5 and the literature[29,30,32]) relaxation times longer than the transport relaxation times are observed, scattering processes with phonons or electrons must reduce the ballistic transport effectively. This agrees well with numerical calculations, which showed that secondary electrons dominate the 2PPE spectra at intermediate-state energies below 0.5 eV (assuming $h\nu > 3$ eV).[11]

Ogawa *et al.*[31] performed autocorrelation experiments on all three low-index copper surfaces using a laser pulse width of 15 fs. At an intermediate-state energy of $E_{int} = 2.5$ eV, where Auger excitation most probably plays only a minor role (see discussion in Sec. V B), it was observed that the relaxation on the $\langle 110 \rangle$ face is the fastest (~ 8 fs) followed by the $\langle 100 \rangle$ face (~ 14 fs) and the $\langle 111 \rangle$ face (~ 20 fs). Simulations using the same pulse width at the same E_{int} yield transport relaxation times of 47 fs for the $\langle 111 \rangle$ face, 43 fs for the $\langle 100 \rangle$ face, and 32 fs for the $\langle 110 \rangle$ face. (These transport relaxation times are smaller compared to the ones for a pulse width of 50 fs, which can be explained by the larger fast component in the autocorrelation in case of the latter.) At this intermediate-state energy, the experimentally derived relaxation times on the low-index copper surfaces show the same pronounced crystal face dependence as in our simulation. The ballistic transport, which is different for the three surfaces due to the different velocity distributions, might therefore be the origin of the observed crystal face dependence of the relaxation times.

At lower intermediate-state energies ($E_{int} = 1.5$ eV), however, the experimentally observed crystal face dependence is reversed, whereas our simulation predicts only a weak dependence on intermediate-state energy. At this intermediate-state energy, however, the observed relaxation times are as long as 66 fs [for Cu(110) (Ref. 31)]. Applying Matthiessen's rule, these values would lead to unrealistically long electron lifetimes. We therefore conclude that either the transport effect is strongly reduced by multiple elastic scattering events or that most of the electrons are excited via Auger decay of d-band holes. The lifetime of the d-band holes, which have practically no transport effect (due to the low dispersion of the d bands), would then be included in these long relaxation times. Note that in contrast to interband transitions the Auger excitation probability depends on intermediate-state energy (low E_{int} is favored).

One way of quantifying experimentally the influence of the transport effect on the relaxation times is to carry out correlation experiments on thin films with variable thickness as demonstrated by Aeschlimann *et al.*[28] and Pawlik.[60] For sufficiently thin films ($\sim$penetration depth of the light), the transport effect is eliminated. It was observed that especially at lower intermediate-state energies (for longer τ_r) the relaxation times for a thin silver film (15 nm) are up to 75% higher than for a thicker film of 30 nm.[28] The magnitude of the transport effect agrees well with the predictions based on our simulation. However, thin films might have a high density of defects, which would increase the elastic scattering rate compared to a single crystal. Since elastic scattering processes compensate the transport effect to a certain extent (see Fig. 10), a comparison of experiments on thin films with the ones on single crystals is difficult.

VI. SUMMARY

In this paper the excitation mechanisms in 2PPE and the ballistic transport for hot electrons in copper are discussed and compared with the experimentally observed electron dynamics.

As for copper, the generation of d-band holes consumes about 70% of the absorbed pump pulse energy (for $h\nu = 3.6$ eV), it is evident that the relaxation of these d-band holes influences the generation and relaxation dynamics of the hot electron distribution. In order to account for the experimental findings, we propose that hot electrons excited via a d-band hole decay dominate the 2PPE spectra for certain intermediate-state energies, where the competing excitation pathway via indirect intraband transitions has only a small probability. As the relaxation dynamics for electrons, which are excited via hole decay, also accounts for the hole lifetime, longer relaxation times compared to electrons excited via direct (or indirect) transitions are observed.

From the difference in the relaxation time for these two excitation pathways, we estimate the lifetime of an upper d-band hole as $\tau_h = 35$ fs. It was found that the lifetime of an

electron in the sp band is by more than factor of 2 shorter than the lifetime of a d-band hole at an excess energy of 2 eV. This difference in lifetime might be due to the strong localization of the d-band hole compared to the sp-band electron, since localization most likely reduces the probability of scattering events.

Due to the projected band gap on Cu(111), the hot electron distribution observed at $k_{\|}=0$ in a 2PPE experiment can only be rationalized by scattering events in the final state. As these additional scatterings diminish the probability of detecting a hot electron, two-photon transitions from initial states with high density of states (d bands) are also observed in the 2PPE spectra. These instantaneous two-photon transitions were identified in a time-resolved correlation experiment, since the corresponding 2PPE intensity was found to follow the autocorrelation function of the laser pulses.

The influence of the ballistic electron transport on the excited electron population in the near-surface region was simulated for all three low-index copper surfaces from the crystal-face-dependent velocity distributions, which were derived from the calculated band structure of copper. It was found that half of the excited electron population is removed within 20 fs and that the ballistic transport is also dependent on the crystal face. The experimentally observed crystal face dependence of the relaxation times[31] is qualitatively reproduced by our simulation. As the observed long relaxation times at small intermediate-state energies ($E_{\mathrm{int}}<0.6$ eV) contradict the predictions of the simulation, we conclude that the generation of secondary electrons and quasielastic scattering must effectively compensate the transport effect. Due to the transport effect, the delayed excitation via hole decay, and the generation of secondary electrons through inelastic scattering, the experimentally observed electron relaxation times do not represent the pure electronic lifetimes, although the energy-dependent hot electron lifetime for inelastic e-e scattering is the dominant quantity in the relaxation dynamics.

ACKNOWLEDGMENTS

We are greatful to Gerhard Ertl for his continuous support. We would like to thank Martin Aeschlimann and Susanne Pawlik for valuable discussions, Bernd Burfeindt for his experimental expertise, and Georg Neuhold for his computational help in the band structure calculation.

[1] J. W. Gadzuk, in *Laser Spectroscopy and Photochemistry on Metal Surfaces*, edited by P. Halevi (World Scientific, Singapore, 1995), p. 897.
[2] F. Weik, A. d. Meijere, and E. Hasselbrink, J. Chem. Phys. **99**, 682 (1993).
[3] X.-L. Zhou, X.-Y. Zhu, and J. M. White, Surf. Sci. Rep. **13**, 73 (1991).
[4] D. Menzel and R. Gomer, J. Chem. Phys. **41**, 3311 (1964).
[5] P. A. Redhead, Can. J. Phys. **42**, 886 (1964).
[6] P. R. Antoniewicz, Phys. Rev. B **21**, 3811 (1980).
[7] P. D. Dederichs, in *Numerical Data and Functional Relationships in Science and Technology*, edited by K.-H. Hellweye and J. L. Olsen, Landolt-Börnstein, New Series, Group III, Vol. 13, Pt. a (Springer-Verlag, Berlin, 1981).
[8] P. Brüesch, *Phonons: Theory and experiments II* (Springer-Verlag, Berlin, 1986).
[9] D. Pine and P. Nozieres, *The Theory of Quantum Liquids* (Benjamin, New York, 1966).
[10] J. J. Quinn, Phys. Rev. **126**, 1453 (1962).
[11] E. Knoesel, A. Hotzel, T. Hertel, M. Wolf, and G. Ertl, Surf. Sci. **368**, 76 (1996).
[12] J. A. Misewich, T. F. Heinz, P. Weigand, and A. Kalamarides, in *Laser Spectroscopy and Photochemistry on Metal Surfaces*, edited by H.-L. Dai and W. Ho (World Scientific, Singapore, 1995), p. 764.
[13] S. I. Anisimov, B. L. Kapeliovich, and T. L. Perel'man, Sov. Phys. JETP **39**, 375 (1974).
[14] R. W. Schoenlein, W. Z. Lin, J. G. Fujimoto, and G. L. Eesley, Phys. Rev. Lett. **58**, 1680 (1987).
[15] G. L. Eesley, Phys. Rev. **33**, 2144 (1986).
[16] C. Suárez, W. E. Bron, and T. Juhasz, Phys. Rev. Lett. **75**, 4536 (1995).
[17] R. H. M. Groeneveld and R. Sprik, Phys. Rev. Lett. **64**, 784 (1990).
[18] R. H. M. Groeneveld, R. Sprik, and A. Lagendijk, Phys. Rev. B **45**, 5079 (1992).
[19] J. M. Hicks, L. E. Urbach, E. W. Plummer, and H.-L. Dai, Phys. Rev. Lett. **61**, 2588 (1988).
[20] J. Hohlfeld, U. Conrad, and E. Matthias, Appl. Phys. B: Lasers Opt. **63**, 541 (1996).
[21] W. S. Fann, R. Storz, H. W. K. Tom, and J. Bokor, Phys. Rev. Lett. **68**, 2834 (1992).
[22] W. S. Fann, R. Storz, H. W. K. Tom, and J. Bokor, Phys. Rev. B **46**, 13 592 (1992).
[23] J. A. Prybyla, H. W. Tom, and G. D. Aumiller, Phys. Rev. Lett. **68**, 503 (1992).
[24] F.-J. Kao, D. G. Busch, D. Gomes da Costa, and W. Ho, Phys. Rev. Lett. **70**, 4098 (1993).
[25] S. Deliwala, R. J. Finlay, J. R. Goldman, T. H. Her, W. D. Mieher, and E. Mazur, Chem. Phys. Lett. **242**, 617 (1995).
[26] J. A. Misewich, T. F. Heinz, and D. M. Newns, Phys. Rev. Lett. **68**, 3737 (1992).
[27] C. A. Schmuttenmaer, M. Aeschlimann, H. E. Elsayed-Ali, R. J. D. Miller, D. A. Mantell, J. Cao, and Y. Gao, Phys. Rev. B **50**, 8957 (1994).
[28] M. Aeschlimann, M. Bauer, and S. Pawlik, Chem. Phys. **205**, 127 (1996).
[29] T. Hertel, E. Knoesel, M. Wolf, and G. Ertl, Phys. Rev. Lett. **76**, 535 (1996).
[30] S. Pawlik, M. Bauer, and M. Aeschlimann, Surf. Sci. **377-379**, 206 (1997).
[31] S. Ogawa, H. Nagano, and H. Petek, Phys. Rev. B **55**, 10 869 (1997).
[32] J. Cao, Y. Gao, R. J. Miller, H. E. Elsayed, and D. A. Mantell, Phys. Rev. B **56**, 1099 (1997).
[33] S. Pawlik, M. Bauer, and M. Aeschlimann, in *Femtochemistry*, edited by M. Chergui (World Scientific, Lausanne, 1995), p. 479.
[34] R. Haight, Surf. Sci. Rep. **21**, 275 (1995).

[35] T. Fauster and W. Steinmann, in *Electromagnetic Waves: Recent Developments in Research*, edited by P. Halevi (Elsevier, Amsterdam, 1995), p. 350.
[36] E. Knoesel, A. Hotzel, and M. Wolf, J. Electron Spectrosc. Relat. Phenom. (to be published).
[37] C. B. Harris, J. D. Neill, N.-H. Ge, R. E. Jordan, J. R. L. Jingle, and C. M. Wong, in *Ultrafast Phenomena*, edited by X P. F. Barbara, J. G. Fujimoto, W. H. Knox, and W. Zinth, Springer Series in Chemical Physics Vol. 62 (Springer-Verlag, Berlin, 1996), p. 445.
[38] M. Wolf, E. Knoesel, and T. Hertel, Phys. Rev. B **54**, 5295 (1996).
[39] U. Höfer, I. L. Shumay, K. L. Kompa, C. Reuss, U. Thomann, W. Wallauer, and T. Fauster, Science **277**, 1480 (1997).
[40] E. Knoesel, T. Hertel, M. Wolf, and G. Ertl, Chem. Phys. Lett. **240**, 409 (1995).
[41] M. Bauer, S. Pawlik, and M. Aeschlimann, Phys. Rev. B **55**, 10 040 (1997).
[42] A. Hotzel, K. Ishioka, E. Knoesel, M. Wolf, and G. Ertl, Chem. Phys. Lett. **285**, 271 (1998).
[43] H. Eckhardt, L. Fritsche, and J. Noffke, J. Phys. F **14**, 97 (1984).
[44] M. K. Reed, M. S. Armas, M. K. Steiner-Shephard, and D. K. Negus, Opt. Lett. **20**, 605 (1995).
[45] M. Nakazawa, T. Nakashima, H. Kubota, and S. Seikai, J. Opt. Soc. Am. B **5**, 215 (1988).
[46] T. Hertel, M. Wolf, and G. Ertl, J. Chem. Phys. **102**, 3414 (1995).
[47] C. A. Schmuttenmaer, C. C. Miller, J. W. Herman, J. Cao, D. A. Mantell, Y. Gao, and R. J. D. Miller, Chem. Phys. **205**, 91 (1996).
[48] M. Aeschlimann, Habilitation thesis, ETH Zürich, 1996.
[49] P. B. Johnson and R. W. Christy, Phys. Rev. B **6**, 4370 (1972).
[50] M. Perner, P. Bost, U. Lemmer, G. V. Plessen, J. Feldmann, U. Becker, M. Mennig, M. Schmitt, and H. Schmidt, Phys. Rev. Lett. **78**, 2192 (1996).
[51] R. Matzdorf, R. Paniago, G. Meister, and A. Goldmann, Solid State Commun. **92**, 839 (1994).
[52] A. Zangwill, *Physics at Surfaces* (Cambridge University Press, Cambridge, England, 1988).
[53] B. Lengeler, in *Electronic Structure of Noble Metals, and Polariton-Mediated Light Scattering*, edited by G. Höhler, Springer Tracts in Modern Physics 82 (Springer-Verlag, Heidelberg, 1978), p. 1.
[54] C. Y. Fong and M. L. Cohen, Phys. Rev. Lett. **24**, 306 (1970).
[55] G. Neuhold, Ph.D. thesis, Freie Universität Berlin, 1997.
[56] C. Y. Fong, J. P. Walter, and M. L. Cohen, Phys. Rev. B **11**, 2759 (1975).
[57] C. Kittel, *Introduction to Solid State Physics* (Wiley, New York, 1986).
[58] M. J. G. Lee, Phys. Rev. B **2**, 250 (1970).
[59] E. Knoesel, Ph.D. thesis, Freie Universität Berlin, 1997.
[60] S. Pawlik (private communication).